HHS Public Access

Author manuscript

Magn Reson Med. Author manuscript; available in PMC 2020 June 01.

Published in final edited form as:

Magn Reson Med. 2019 June ; 81(6): 3567–3577. doi:10.1002/mrm.27669.

Absolute Quantitative MR Perfusion and Comparison against Stable-Isotope Microspheres

Mr. Yong I. Jeong, MS[1], **Dr. Gregory A. Christoforidis, MD**[2], **Dr. Niloufar Saadat, MD**[2], **Dr. Keigo Kawaji, PhD**[2,3,4], **Dr. Charles G. Cantrell, PhD**[2], **Dr. Steven Roth, MD**[5], **Dr. Marek Niekrasz, DVM**[6], and **Dr. Timothy J. Carroll, PhD**[2]

[1]Department of Biomedical Engineering, Northwestern University, Evanston, IL, USA

[2]Department of Radiology, University of Chicago, Chicago, IL, USA

[3]Department of Biomedical Engineering, Illinois Institute of Technology, Chicago, IL, USA

[4]Department of Medicine, University of Chicago, Chicago, IL, USA

[5]Department of Anesthesiology, University of Illinois, College of Medicine, Chicago, IL, USA

[6]Department of Surgery, University of Chicago, Chicago, IL, USA

Abstract

Purpose: This work sought to compare a quantitative T_1 bookend DSC MRI based perfusion protocol for absolute cerebral blood flow (qCBF) against CBF measured by the stable-isotope neutron capture microsphere method, a recognized reference standard for measuring tissue blood flow, at normocapnia, hypercapnia and in acute stroke.

Methods: CBF was measured in anesthetized female canines by MRI and microspheres over two consecutive days for each case. On day 1, five canines were measured before and during a physiological challenge induced by carbogen inhalation, and on day 2 four canines were measured following permanent occlusion of the middle cerebral artery (MCAO). CBF and cerebrovascular reactivity (CVR) measured by MRI and microsphere deposition were compared.

Results: MRI correlated strongly with microspheres at the hemispheric level for CBF during normo-and hypercapnic states ($r^2 = 0.96$), for individual CVR ($r^2 = 0.84$), and for post-occlusion CBF ($r^2 = 0.82$). Correction for the delay and dispersion of the contrast bolus resulted in a significant improvement in the correlation between MRI and microsphere deposition in the ischemic state ($r^2 = 0.96$). In all comparisons, moderate correlations were found at the regional level.

Conclusion: In an experimental canine model with and without permanent MCAO, MRI-based qCBF yielded moderate to strong correlations for absolute quantitative CBF and CVR measurements during normocapnia and hypercapnia. Correction for delay and dispersion greatly improved the quantitation during MCAO, underscoring the importance for this correction under focal ischemic condition.

CORRESPONDING AUTHOR: Dr. Gregory A. Christoforidis, MD, University of Chicago Hospitals, Department of Radiology, 5841 South Maryland Avenue, Chicago, IL 60637, gchristoforidis@radiology.bsd.uchicago.edu, Phone: +1 773 7026339, Fax: +1 773 702 1161.

Keywords

acute stroke; cerebral blood flow; cerebrovascular reactivity; dynamic susceptibility contrast; microspheres; MRI

INTRODUCTION

The successful DEFUSE-3 and associated American Heart/Stroke Association recommendations have sparked new interest in tissue-based selection criteria to allow for a greater number of stroke patients to be safely treated. It is well known that both the degree of hypoperfusion (in ml/100 g/min) as well as the duration of hypoperfusion determine the infarct volume and growth rate (1). Results from the DAWN (DWI or CTP Assessment with Clinical Mismatch in the Triage of Wake-Up and Late Presenting Strokes Undergoing Neurointervention with Trevo) trial (2) and DEFUSE-3 trial (Endovascular Therapy Following Imaging Evaluation for Ischemic Stroke) (3) suggest that perfusion imaging in the workup of acute ischemic stroke is critical. Therefore, there is an unmet need for a quantitative measure of tissue perfusion that can be integrated into a clinically feasible perfusion-diffusion scan protocol. This work attempts to determine the degree to which a next generation quantitative perfusion imaging method agrees with reference standard values under a variety of physiologic conditions. Because dynamic susceptibility contrast (DSC) MRI perfusion depends on an arterial input function proximal to the occlusion site, cerebral blood flow in the setting of ischemia presents the additional challenge of incorporating the effect of delay and dispersion when assessing cerebral blood flow (4). As a result, we sought to measure CBF both in the normal state and during ischemic conditions. In this study we compare a previously reported means for quantifying cerebral blood flow (qCBF) by MRI against the reference standard stable-isotope neutron capture microsphere deposition in a controlled experimental model of ischemic stroke, as well as quantifying cerebrovascular reactivity (CVR) using CO_2 challenge.

An endovascular canine model provides numerous advantages as a translational model for the assessment of perfusion imaging studies. Dogs have a highly evolved gyrencephalic neocortex with a ratio of white to gray matter that more closely approximates that in humans relative to small animal models (5,6). Indeed, comparative anatomic studies across vertebrate species indicate that the pial network organization along the forebrain of canines is more comparable to primates than that of other animals (7). Second, dogs provide the necessary tissue volumes to simultaneously evaluate the core and penumbra during ischemia (8–11). Third, the variability in collateral circulation in mongrel dogs allows for an array of varying penumbra zones suitable for the current study. Fourth, the neurovascular architecture, including the size of the vessels, symmetry and lack of rete mirabile in dogs accommodates an array of endovascular devices and interventional radiology techniques, permitting a minimally invasive approach to the surgery while providing real-time visualization of occlusion. Fifth, the proposed method of MCA occlusion in dogs offers a relatively inexpensive alternative to nonhuman primate models of acute focal ischemia (12,13). Sixth, cerebrovascular reactivity in canines is similar to that of humans. Finally,

endovascular MCA occlusion prevents imaging artifacts and traumatic cerebrovascular reaction introduced by open surgical occlusion.

METHODS

The experimental protocol was approved by the University of Chicago Institutional Animal Care and Use Committee, and is reported in compliance with ARRIVE guidelines. The University of Chicago is an AAALAC International accredited institution adhering to the following guidelines, regulations and policies: a) Guide for the Care and Use of Laboratory Animals (National Research Council), b) USDA Animal Welfare Act and Animal Welfare Regulations, and c) Public Health Service Policy on Humane Care and Use of Laboratory Animals.

Nine female, mongrel canines were recruited for this study, of which the last four experiments could not be included. Technical problems within the protocol arose in two of the four, where data could not be collected for analysis because of a scanner failure and a missing perfusion scan due to technician error. In the other two cases, physiological instability during the collection of the perfusion data and microspheres did not allow for a controlled comparison of MR and microsphere values. Large amount of air was inadvertently introduced inside a blood vessel during an injection of microspheres in one case, and in the other case, unstable $PaCO_2$ values were seen throughout the experiment and a different carbogen was used (10% instead of 5% CO_2). These animals also died before completion of the experiment. In total, five female, mongrel canines (mean ± standard deviation of weight: 28.2 ± 3.38 kg; age: 76.8 ± 6.97 months) were studied successfully on day 1, and four of the five were studied on day 2. One animal could not be studied on day 2 due to a vessel perforation during the occlusion of middle cerebral artery (Figure 1).

Animals included were purpose bred, research naïve and purchased from Class A dealers of conventional health status. They were offered social housing opportunities with wood shaving bedding and one cage companion in oversized enclosures that exceed the requirements of the Animal Welfare Act. 12/12 light cycles were provided, and temperatures were consistent with the Guide for the Care and Use of Laboratory Animals recommendations. The animals were offered species specific environmental enrichment, and were given daily opportunities to exercise while the enclosures were cleaned. Animals were fed species specific commercial diet (Teklad: Certified Lab Dog Diet), and were visually inspected on a daily basis by the husbandry and veterinary staffs.

Experiment Procedure

Experiments were performed on two consecutive days according to the timeline shown in Figure 1. On day 1, qCBF images were acquired simultaneously with microsphere injection during normocapnia (target $PaCO_2$ range 30–40 mmHg using room air) and during hypercapnia (target $PaCO_2$ range > 60 mmHg induced by carbogen gas inhalation (5% CO_2/95% O_2)). On day 2 of the study, four of the five animals underwent permanent endovascular middle cerebral artery occlusion (MCAO) at the M1 segment (1) while in a normocapnic state. One animal was not imaged on day 2 due to an unanticipated vessel perforation during MCAO, following which the animal was euthanized.

Anesthesia was maintained using isoflurane (1% end-tidal, 0.75 MAC (minimum alveolar concentration for dogs)), continuous propofol infusion (100–200 μg/kg/min) and intravenous rocuronium (0.4–0.6 mg/kg every 10–30 minutes titrated to effect). These anesthetics were selected to minimize influence upon cerebrovascular reactivity. Physiologic monitoring included: invasive blood pressure, end-tidal CO_2, O_2 saturation, rectal temperature, heart rate, cardiac rhythm, arterial blood gases, glucose, electrolytes, and hematocrit.

On day 1, a 5-F sheath was placed in the right common femoral artery for arterial blood pressure monitoring and arterial blood gas determinations. A 3-F pigtail catheter was advanced via the same sheath into the left cardiac ventricle for microsphere injection. The animal was then transported to the MRI unit. After completion of the MRI scans, the sheath was removed, and hemostasis was achieved. On day 2, the animal was brought back to the angiography suite where the right middle cerebral artery was accessed endovascularly using fluoroscopic guidance as previously described (1,14). MCAO was verified by selective ipsilateral and contralateral internal carotid and vertebral arteriography (OEC9800, General Electric Healthcare, Chicago, IL, USA). Throughout the experiments, physiologic parameters were maintained within normal range with the exception of $PaCO_2$ for hypercapnic state.

MRI Scan Protocol

All MRI images were acquired on a 3T magnet (Achieva, Philips Healthcare, Best, Netherlands). Animals were placed in the head first, prone position within a 15-channel receive-only head coil. qCBF scans were reported in ml/100 g/min using a previously reported “bookend DSC MRI perfusion” approach (15–17), which uses pre- and post-contrast T_1 maps bookended to the DSC MRI perfusion sequence to calculate parenchymal T_1 changes and calibrate the DSC scan for quantitative perfusion (Figure 1). The T_1 maps were derived using a scan protocol consisting of a 2D EPI Look-Locker inversion recovery (FOV/Matrix = 220 mm/224, Slice Thickness = 4 mm, single slice) with variable delay time and DSC perfusion (FOV/Matrix = 220 mm/224, single shot, EPI, Fat Saturated, No. of slices = 5, Slice Thickness = 6 mm, TR/TE = 315/40, Flip angle = 75°, 200 time points). A gadolinium-based contrast agent (Multihance, Bracco, Princeton, NJ, USA) was injected followed by a saline flush (Gadolinium: single dose 3 ml at 2 ml/sec, saline: 20 ml at 2 ml/sec).

Microsphere Injection Protocol

Microspheres were injected within 2 minutes of the acquisition of the quantitative perfusion images while the animal was kept motionless in the MR scanner. Each injection consisted of 4 ml of 10^7 stable-isotope labeled 15-μm microspheres (STERIspheres, BioPal Inc, Medford, MA, USA) into the left ventricle over 10 seconds using the previously placed 3-F pigtail catheter. Positioning in the left ventricle was confirmed by both pressure waveform and x-ray. Reference blood was collected from the abdominal aorta using a catheter connected to an MRI compatible withdrawal/infusion pump (PHD 2000, Harvard Apparatus, Holliston, MA, USA). The blood withdrawal was initiated 10 seconds prior to the microsphere injection. A total of 20 ml of blood at 10 ml/min was withdrawn for analysis.

Gold, samarium, and lutetium stable-isotope labeled microspheres were used for normocapnia, hypercapnia, and post-MCAO respectively.

The brains were excised, sectioned, photographed, weighed wet and placed in a drying oven (Model 20 Lab Oven, Quincy lab, Inc, Chicago, IL, USA) prior to microsphere analysis. Three contiguous 6 mm thick sections at and posterior to the MCA were cut using a calibrated brain cutting matrix (Canine Brain Matrix, Stoelting Co., Wood Dale, IL, USA). Slice thickness equaled that of the 2D MRI slices used for perfusion. Each slice was sectioned into eight regions (inferior, middle, superior, and basal for left and right). Microsphere deposition was analyzed in each region via neutron activation (18) by BioPAL Inc. (Medford, MA, USA) and reported in ml/g/min. The calculation was:

$$CBF = \frac{N_t R_b}{N_b m_t} \quad (1)$$

where N_t is the microsphere counts in the tissue sample in decays per minute (dpm), N_b is the microsphere counts in the reference blood draw, R_b is the rate of reference blood withdrawal (ml/min) and m_t is the mass of the tissue sample (grams). The CBF measured using neutron activation of stable-isotope labeled microspheres had been previously reported to have a high correlation ($r > 0.95$) to CBF by traditional radiolabeled microspheres, and the type of microsphere was found to have no effect on CBF measurements (19).

Data Analysis

The MRI perfusion images were post-processed to create qCBF (in ml/100 g/min) parametric images for normocapnia, hypercapnia, and post-MCAO based on techniques previously reported (4,15–17,20,21) using custom made post-processing code created on MATLAB v9.3 (The Mathworks, Natick, MA, USA). The arterial input function (AIF) was chosen automatically based on a simultaneous assessment of early arrival time, narrow bolus, and large area under the concentration curve (large blood volume in the voxel) based on a prior study (20). The AIF was then fitted to a gamma-variate model and was resampled depending on the image slice of interest to derive quantitative maps (4).

To correct for the delay and dispersion effects, the gadolinium bolus arrival time in the tissue was calculated relative to that of the AIF (4). The dispersion of the bolus, per unit time, was determined by comparing the bolus shape of the AIF to that of the venous outflow measured at the sagittal sinus, which arrives 2–3 seconds later than the AIF. The strength of the bolus dispersion, β, was calculated on a case by case basis using linear time invariant system theory and modelling the impulse response function of the tissue vasculature as an exponential (4):

$$VOF(t + t_D) = \frac{\alpha}{t_D + 1} \cdot e^{-\beta \cdot \frac{t}{t_D}} \otimes AIF(t) \quad (2)$$

where t_D is the measured delay time between the bolus in the AIF and the venous output function (VOF), and α and β are fitted coefficients. The VOF was chosen manually by looking for large T_1 differences (before and after contrast agent) and confirming anatomically. Then the local AIF of a voxel of tissue with delayed arrival $t_T (0 < t_T < t_D)$ was simply calculated as:

$$AIF_{DD}(t) = AIF(t) \otimes \left(\frac{\alpha}{t_T + 1} \cdot e^{-\beta \cdot \frac{t}{t_T}}\right) \quad (3)$$

to describe the dispersed shape of the "local AIF" with a delayed arrival time of t_T at the tissue. The local AIF was then used for deconvolution analysis (i.e. singular value decomposition) with delay-shifted tissue concentration curves to derive maps of CBV, CBF and MTT.

Aside from the delay and dispersion effects, DSC perfusion is sensitive to the scaling of the AIF; therefore, a calibration was added using steady-state CBV. Steady-state CBV, calculated using T_1 maps before and after a contrast agent injection, has been shown to provide better measurements than DSC CBV (22,23). Then, we applied a correction factor to account for the effects of water exchange from the intra- to extravascular space as previously described (21), since water exchange is known to cause an error in the steady-state CBV if data are not properly corrected by a water exchange correction factor (WCF) (21,24,25). The resulting expression for qCBF was:

$$qCBF = \frac{1}{\rho} \cdot \frac{1 - Hct_{LV}}{1 - Hct_{SV}} \cdot CBF_{DSC} \cdot \frac{CBV_{SS,WM}}{CBV_{DSC,WM}} \cdot WCF \quad (4)$$

where CBF_{DSC} is the CBF calculated from the DSC images, $CBV_{DSC,WM}$ is the average white matter CBV from the DSC images, $CBV_{SS,WM}$ is the average white matter steady-state CBV quantified using the T_1 maps, and WCF is the water exchange correction factor, ρ is the average density of brain tissue (1.04 g/ml), and Hct_{LV} and Hct_{SV} are the hematocrit levels in large (0.45) and small vessels (0.25), respectively. For the calculation of CVR, which requires two gadolinium injections, two WCFs were determined to account for the residual gadolinium in the blood pool arising from the back-to-back perfusion scans. The water exchange correction factor for first injection (WCF_1) and for second injection (WCF_2), based on method previously described (21), were:

$$WCF_1 = 0.35\ \Delta R_1^2 + 0.11\ \Delta R_1 + 0.06 \quad (5)$$

$$WCF_2 = 0.22\ \Delta R_1^2 + 2 \cdot 10^{-6}\ \Delta R_1 + 0.49 \quad (6)$$

as a function of the change in R_1 ($1/T_1$) of blood.

ROIs were manually drawn by a trained operator (YIJ) and reviewed by an interventional neuroradiologist with 12 years of experience in the evaluation of canine MRI (GAC) on the pre-contrast DSC images (not the post-processed qCBF images) to closely match the previously mentioned sectioned-regions of the brain. Both operators (YIJ and GAC), who were blinded to both MR-qCBF values and the microsphere values, placed ROIs based on the pre-contrast T_2*-weighted MRI images and photographs of the tissue sections that were taken at the time of sectioning. The operator relied on the proportional size of the brain sections to the whole brain slice, and any visible anatomical cues, such as white matter and sulcal markings (Figure 2). MRI regions of interest were applied as masks to the quantitative perfusion images to calculate mean values corresponding to each ROI. MR-qCBF values were compared to microsphere-qCBF by hemispheric and regional averages using linear regression analysis to test the hypothesis that MRI perfusion correlates strongly with reference standard microsphere deposition. CVR for each method was measured as the percent change in perfusion per change in partial pressure of CO_2 measured in the arterial blood samples:

$$CVR(\%) = \frac{\frac{qCBF_{post} - qCBF_{pre}}{qCBF_{pre}}}{\Delta\, PaCO_2} \cdot 100 \quad (7)$$

and analyzed using linear regression plots. For each linear regression analysis, the slope, intercept, coefficient of determination (r^2), *P*-value, and 95% confidence intervals were reported. After the requisite anatomic survey, arterial blood gas, MRI perfusion scans and microsphere injections were performed within 2 minutes of each other while maintaining a stable end-tidal CO_2.

RESULTS

Detailed results of the linear regression analyses are shown in Table 1. Regional (ROI-by-ROI) and values averaged over the entire hemisphere were compared between MR-qCBF and microsphere-qCBF from day 1 (Figure 3). The quantitative comparison between hemispheric average qCBF values (Figure 3A) showed a strong correlation ($r^2 = 0.96$), while a poorer correlation was seen for regional comparison ($r^2 = 0.82$). CVR comparison (Figure 3B) resulted in a similar correlation, but with a lower r^2 coefficient for both hemispheric ($r^2 = 0.84$) and regional comparisons ($r^2 = 0.61$). In general, the correlation was not as strong when measuring CVR as compared to qCBF. Bland-Altman plots were also calculated for qCBF (Figure 3C) and CVR (Figure 3D). In general, low bias but wide scatter was found.

Quantitative CBF in normocapnia and hypercapnia were compared by linear regression analysis against arterial $PaCO_2$ (Figure 4). Both MR and microsphere qCBF values exhibited a statistically significant linear correlation ($r^2 = 0.70$ and $r^2 = 0.72$ respectively) as expected of the vasodilatory effects.

Post-occlusion perfusion from day 2 compared MRI and microsphere methods (Figure 5). A strong linear correlation was found for hemisphere averages (r^2 = 0.82), while a mediocre correlation was found for regional averages (r^2 = 0.54) (Figure 5A). Correction for delay and dispersion resulted in an improvement in the correlation between qCBF and microsphere deposition in the ischemic state for hemisphere averages (r^2 = 0.96), but not so much for regional averages (r^2 = 0.55) (Figure 5B). The correction also brought the slope of the linear regression much closer to the line of unity for both the hemispheric (0.80 to 0.97) and regional comparison (0.74 to 0.93) (Table 1). In the Bland-Altman analysis (Figure 5C and Figure 5D), bias was reduced closer to zero after correction at the regional and hemispheric level. But high variability was still seen for regional differences.

A summary of values including average whole-brain MR-qCBF at baseline and at normocapnia, MR-CVR, microsphere-qCBF, microsphere-CVR, and $PaCO_2$ were obtained for each case and are reported in Table 2. Representative slices at normocapnia, hypercapnia, and during MCAO are shown in Figure 6. The corresponding DWI image, acquired at 2 hours post coil deployment, is shown for reference. Visual inspection of perfusion images at normocapnia and hypercapnia demonstrates qualitatively the expected global increase of perfusion associated with a greater arterial CO_2 concentration.

DISCUSSION

In this study, we found that quantitative MR perfusion based on a previously reported protocol (15–17) correlated to the reference standard microsphere deposition values over a range of physiologic conditions. Strong correlations were observed for hemispheric comparisons under normocapnia and hypercapnia as well as in a setting of acute ischemia resulting from MCAO. Correction for delay and dispersion in the ischemic state improved the correlation. In contrast, weaker correlations were found for regional comparisons. To the best of our knowledge, this is the first demonstration of reference standard cerebral perfusion comparison under three clinically significant hemodynamic conditions (normocapnia, hypercapnia and ischemia due to MCAO).

Microspheres embolize vessels slightly larger than capillaries. Cerebral blood flow is directly proportional to the number of blood vessels within the capillary bed. Reference peripheral arterial blood samples are used to derive absolute blood flow values within a 10% margin of error, given that there is a good mixing of microspheres at the injection site and an abundance of microspheres. Due to the small size of the microspheres, the risk of cerebral infarction is negligible. In addition, the 15-μm microspheres used in this study have been found to be highly reproducible during serial injections with minimal shunting and minimal effect on regional blood flow distributions (26).

Prior studies quantifying CBF by MRI compared MR CBF measurements against PET CBF measurements with varying levels of success. Lin et al. (27) derived a global correction factor by averaging venous output function from healthy volunteers and applied this as a ratio to clinically stable patients with unilateral carotid artery occlusion. This method was used in contrast-enhanced perfusion imaging to achieve an r^2 of 0.64 ($MR = 1.02 * PET + 20.1$). A different study by Vakil et al. (28) used the bookend DSC MR perfusion imaging

on patients with Moyamoya or internal carotid artery occlusions and compared against PET to find a r^2 of 0.66 ($MR = 0.75*PET - 0.89$). Alternatively, Kimura et al. (29) compared continuous arterial spin labeling MR perfusion against PET perfusion in patients with occlusive carotid artery disease and found an average r^2 of 0.50 ($MR = 1.12*PET - 0.47$). Given that microspheres employed in the current study provide gold-standard reference values of CBF, the bookend DSC MR perfusion imaging used in this study (15–17) may be a good alternative for absolute CBF.

Quantitative MR CBF and CVR was found to be highly correlated with microsphere CBF and CVR. There was a good correlation between the two methods for measuring qCBF, but a weaker correlation was found when calculating CVR. This might be caused by error propagation from combining two qCBF measurements (Eq. 7).

The results in this study suggest that delay and dispersion effects play a large role in the quantification of absolute CBF using DSC MRI in the setting of MCAO. The correlation improved at the hemispheric level and brought the linear regression line much closer to the line of unity in both the hemispheric and regional analysis. In the Bland-Altman plot, the bias was reduced much closer to zero, though the variability still remained at large at the regional level. This finding corroborates our prior experience and other studies of dispersion effects in stroke(4,30) and lends support to the importance of accounting for delay and dispersion when assessing cerebral blood flow in ischemic stroke using models that employ arterial input functions.

On the other hand, the delay and dispersion correction seemed to have an effect on the normal hemisphere and decrease CBF in some cases (Figure 5). The MRI acquisition in this study was designed to be more sensitive to delay and dispersion effects. Rather than setting TR to about 1000 – 2000 ms, which are common in the clinical setting, we acquired fewer slices (five) and a much higher frame rate (TR = 315 ms). As such, we were able to “see” ipsilateral delay and dispersion effects in healthy hemisphere. In other words, the vascular transport function from a hypothetical MCA curve (i.e. AIF) to the cerebral penetrating arteries on the surface of the brain. In some cases, the CBF decreased slightly. This may result from the automated AIF selection algorithm, which was not chosen or adjusted manually, and may have a slight admixture of distal signal curves. In other words, MCA territory “AIF” may be contaminated with anterior cerebral artery and posterior cerebral artery components which are already slightly dispersed.

The delay and dispersion model used in this study consisted of a patient specific α and β (Eq. 2), and delay and dispersion were assumed to be directly related. However, in a cross-sectional study over a population of patients (30), large delay with little dispersion or large dispersion with little delay were both observed. This may be because delayed arrival depends more on patient specific physiologic parameters, most notably perfusion pressure, cardiac output, and the age of the patient than on vascular topology. On the other hand, bolus dispersion depends strongly on the topology of the vasculature (arterial diameter, tortuosity, completeness of the Circle of Willis, degree of collateralization, local vasodilation, venous congestion, intracranial pressure, etc). These will also vary patient-to-patient. However,

within a single patient, with fixed vascular topology, the link between bolus dispersion and transit time is more tightly coupled. Hence, patient specific α and β were fitted.

Discrepancies in measuring qCBF by MRI versus microspheres may be the result of ROI selection on the MR DSC images and sectioning artifacts. While the MR time-series was optimized to acquire at high temporal resolution and frame rate to track the bolus, this resulted in lower spatial resolution and susceptibility artifacts prominent in gradient-echo acquisitions. Furthermore, specimen selection and segmentation in fresh brain tissue are prone to artifacts that are especially pronounced in smaller segments versus hemispheric segments. This is also augmented by the brain region cuts consisting of gray matter and white matter that have large differences in CBF. Potentially different proportions of gray matter and white matter resulting from discrepancies in the hand drawn ROIs and excised brain sections likely has had a considerable effect on the ROI averages. Achieving exact ROIs that resemble the actual excised brain sections may lend itself to greater error, leading to greater disparities in the regional comparisons versus the hemispheric comparisons.

This study consisted of the following limitations. First, a larger sample size is warranted for gaining a higher confidence in our results, especially for assessing MR-CVR. Moreover, four cases were removed from analysis due to technical and physiological problems. The technical problems, which precluded collection of data, arose from human error and were not related to the pulse sequence or post-processing methods used. There may have been bias introduced from removing the two cases with physiological problems. However, it was within best reason to exclude the cases, because the air introduced in the blood vessel, the unstable $PaCO_2$, and the different carbogen could have had unpredictable circumstances. Secondly, reducing the artifact-induced variability may yield more precise MR-qCBF and MR-CVR measurements. This could be achieved by further optimizing DSC acquisition parameters and calibration steps to minimize susceptibility artifacts. Lastly, regional comparisons throughout the study were limited by the variability from ROI registration. Therefore, local discrepancies, which would be diluted in the hemispheric comparisons, between the MR and microsphere methods could not be clearly determined.

CONCLUSION

This work showed that T_1-bookended DSC MRI-derived values of CBF and CVR are strongly correlated with reference standard stable-isotope labeled microsphere deposition in the setting of normocapnia, hypercapnia, and ischemia by MCAO. At the regional level, larger variability existed resulting in a moderate correlation. In the MCAO experiment, MR versus microsphere qCBF correlation improved when corrected for the effect of delay and dispersion, underscoring the importance for this type of correction when assessing perfusion in the setting of focal ischemia.

ACKNOWLEDGMENTS

This work was supported by National Institutes of Health Research Grants [R01-NS093908, R21-EB017928]; American Heart Association Research Grant [AHA GRNT-20380798]; and American Heart Association Pre-Doctoral Fellowship [AHA 16PRE27530023].

REFERENCES

1. Christoforidis GA, Vakil P, Ansari SA, Dehkordi FH, Carroll TJ. Impact of Pial Collaterals on Infarct Growth Rate in Experimental Acute Ischemic Stroke. AJNR American journal of neuroradiology 2017;38(2):270–275. [PubMed: 27856435]
2. Nogueira RG, Jadhav AP, Haussen DC, et al. Thrombectomy 6 to 24 Hours after Stroke with a Mismatch between Deficit and Infarct. The New England journal of medicine 2018;378(1):11–21. [PubMed: 29129157]
3. Albers GW, Marks MP, Kemp S, et al. Thrombectomy for Stroke at 6 to 16 Hours with Selection by Perfusion Imaging. The New England journal of medicine 2018.
4. Mouannes-Srour JJ, Shin W, Ansari SA, et al. Correction for arterial-tissue delay and dispersion in absolute quantitative cerebral perfusion DSC MR imaging. Magnetic resonance in medicine 2012;68(2):495–506. [PubMed: 22162092]
5. Zhang K, Sejnowski TJ. A universal scaling law between gray matter and white matter of cerebral cortex. Proc Natl Acad Sci U S A 2000;97(10):5621–5626. [PubMed: 10792049]
6. Traystman RJ. Animal models of focal and global cerebral ischemia. ILAR J 2003;44(2):85–95. [PubMed: 12652003]
7. McHedlishvili G, Kuridze N. The modular organization of the pial arterial system in phylogeny. J Cereb Blood Flow Metab 1984;4(3):391–396. [PubMed: 6332116]
8. Tu YK, Heros RC, Candia G, et al. Isovolemic hemodilution in experimental focal cerebral ischemia. Part 1: Effects on hemodynamics, hemorheology, and intracranial pressure. J Neurosurg 1988;69(1):72–81. [PubMed: 3379478]
9. MOLINARI GF, LAURENT JP. A Classification of Experimental Models of Brain Ischemia. Stroke 1976;7:14–17.
10. Branston NM, Ladds A, Symon L, Wang AD. Comparison of the effects of ischaemia on early components of the somatosensory evoked potential in brainstem, thalamus, and cerebral cortex. J Cereb Blood Flow Metab 1984;4(1):68–81. [PubMed: 6693514]
11. Diaz FG, Ausman JI. Experimental cerebral ischemia. Neurosurgery 1980;6(4):436–445. [PubMed: 6771672]
12. Quigley M Non-human primates: the appropriate subjects of biomedical research? J Med Ethics 2007;33(11):655–658. [PubMed: 17971469]
13. Bhogal N, Hudson M, Balls M, Combes RD. The use of non-human primates in biological and medical research: evidence submitted by FRAME to the Academy of Medical Sciences/Medical Research Council/Royal Society/Wellcome Trust Working Group. Altern Lab Anim 2005;33(5): 519–527. [PubMed: 16268763]
14. Christoforidis GA, Rink C, Kontzialis MS, et al. An endovascular canine middle cerebral artery occlusion model for the study of leptomeningeal collateral recruitment. Investigative radiology 2011;46(1):34–40. [PubMed: 20856126]
15. Carroll TJ, Horowitz S, Shin W, et al. Quantification of cerebral perfusion using the “bookend technique”: an evaluation in CNS tumors. Magn Reson Imaging 2008;26(10):1352–1359. [PubMed: 18538523]
16. Sakaie KE, Shin W, Curtin KR, McCarthy RM, Cashen TA, Carroll TJ. Method for improving the accuracy of quantitative cerebral perfusion imaging. Journal of magnetic resonance imaging : JMRI 2005;21(5):512–519. [PubMed: 15834910]
17. Shin W, Horowitz S, Ragin A, Chen Y, Walker M, Carroll TJ. Quantitative cerebral perfusion using dynamic susceptibility contrast MRI: evaluation of reproducibility and age- and gender-dependence with fully automatic image postprocessing algorithm. Magnetic resonance in medicine 2007;58(6):1232–1241. [PubMed: 17969025]
18. Heydorn K Neutron activation analysis for clinical trace element research Boca Raton, Fla.: CRC Press; 1984.
19. Reinhardt CP, Dalhberg S, Tries MA, Marcel R, Leppo JA. Stable labeled microspheres to measure perfusion: validation of a neutron activation assay technique. Am J Physiol Heart Circ Physiol 2001;280(1):H108–116. [PubMed: 11123224]

20. Carroll TJ, Rowley HA, Haughton VM. Automatic calculation of the arterial input function for cerebral perfusion imaging with MR imaging. Radiology 2003;227(2):593–600. [PubMed: 12663823]

21. Shin W, Cashen TA, Horowitz SW, Sawlani R, Carroll TJ. Quantitative CBV measurement from static T1 changes in tissue and correction for intravascular water exchange. Magnetic resonance in medicine 2006;56(1):138–145. [PubMed: 16767742]

22. Speck O, Chang L, Itti L, Itti E, Ernst T. Comparison of static and dynamic MRI techniques for the measurement of regional cerebral blood volume. Magnetic resonance in medicine 1999;41(6): 1264–1268. [PubMed: 10371461]

23. Lin W, Celik A, Paczynski RP. Regional cerebral blood volume: a comparison of the dynamic imaging and the steady state methods. Journal of magnetic resonance imaging : JMRI 1999;9(1): 44–52. [PubMed: 10030649]

24. Hazlewood CF, Chang DC, Nichols BL, Woessner DE. Nuclear magnetic resonance transverse relaxation times of water protons in skeletal muscle. Biophys J 1974;14(8):583–606. [PubMed: 4853385]

25. Donahue KM, Weisskoff RM, Chesler DA, et al. Improving MR quantification of regional blood volume with intravascular T1 contrast agents: accuracy, precision, and water exchange. Magnetic resonance in medicine 1996;36(6):858–867. [PubMed: 8946351]

26. Marcus ML, Heistad DD, Ehrhardt JC, Abboud FM. Total and regional cerebral blood flow measurement with 7–10-, 15-, 25-, and 50-mum microspheres. J Appl Physiol 1976;40(4):501–507. [PubMed: 931870]

27. Lin W, Celik A, Derdeyn C, et al. Quantitative measurements of cerebral blood flow in patients with unilateral carotid artery occlusion: a PET and MR study. Journal of magnetic resonance imaging : JMRI 2001;14(6):659–667. [PubMed: 11747021]

28. Vakil P, Lee JJ, Mouannes-Srour JJ, Derdeyn CP, Carroll TJ. Cerebrovascular occlusive disease: quantitative cerebral blood flow using dynamic susceptibility contrast mr imaging correlates with quantitative H2[15O] PET. Radiology 2013;266(3):879–886. [PubMed: 23297337]

29. Kimura H, Kado H, Koshimoto Y, Tsuchida T, Yonekura Y, Itoh H. Multislice continuous arterial spin-labeled perfusion MRI in patients with chronic occlusive cerebrovascular disease: a correlative study with CO2 PET validation. Journal of magnetic resonance imaging : JMRI 2005;22(2):189–198. [PubMed: 16028241]

30. Calamante F, Willats L, Gadian DG, Connelly A. Bolus delay and dispersion in perfusion MRI: implications for tissue predictor models in stroke. Magnetic resonance in medicine 2006;55(5): 1180–1185. [PubMed: 16598717]

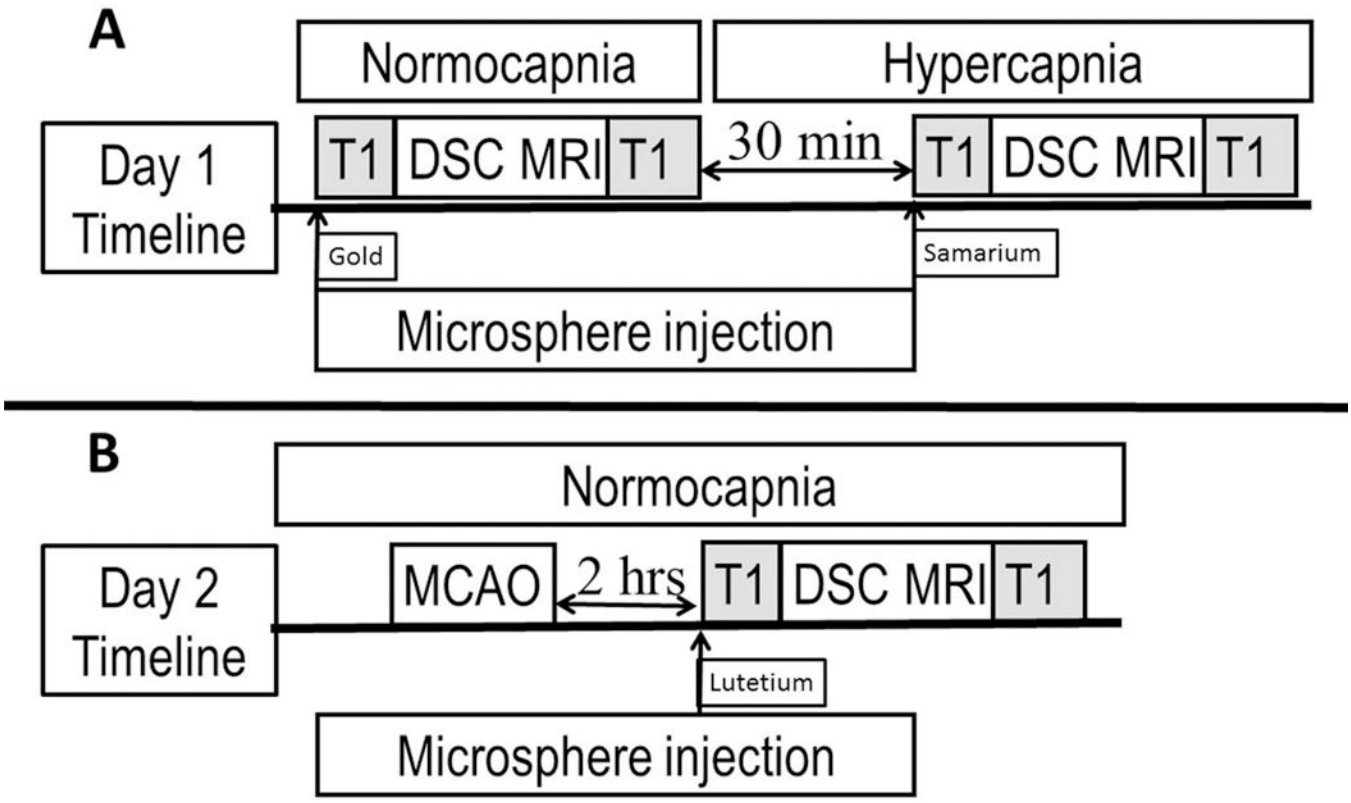

Figure 1.

Timeline for the experimental model. (A) On Day 1, DSC MRI perfusion scans and microsphere injections are performed in normocapnia and hypercapnia (induced via respiration of carbogen gas (5% CO_2/95% O_2). (B) On Day 2, MCAO is induced, and MRI perfusion and microsphere injections are performed. The DSC scans are bookended by Look-Locker T_1 map acquisitions to calibrate CBF for quantitative CBF.

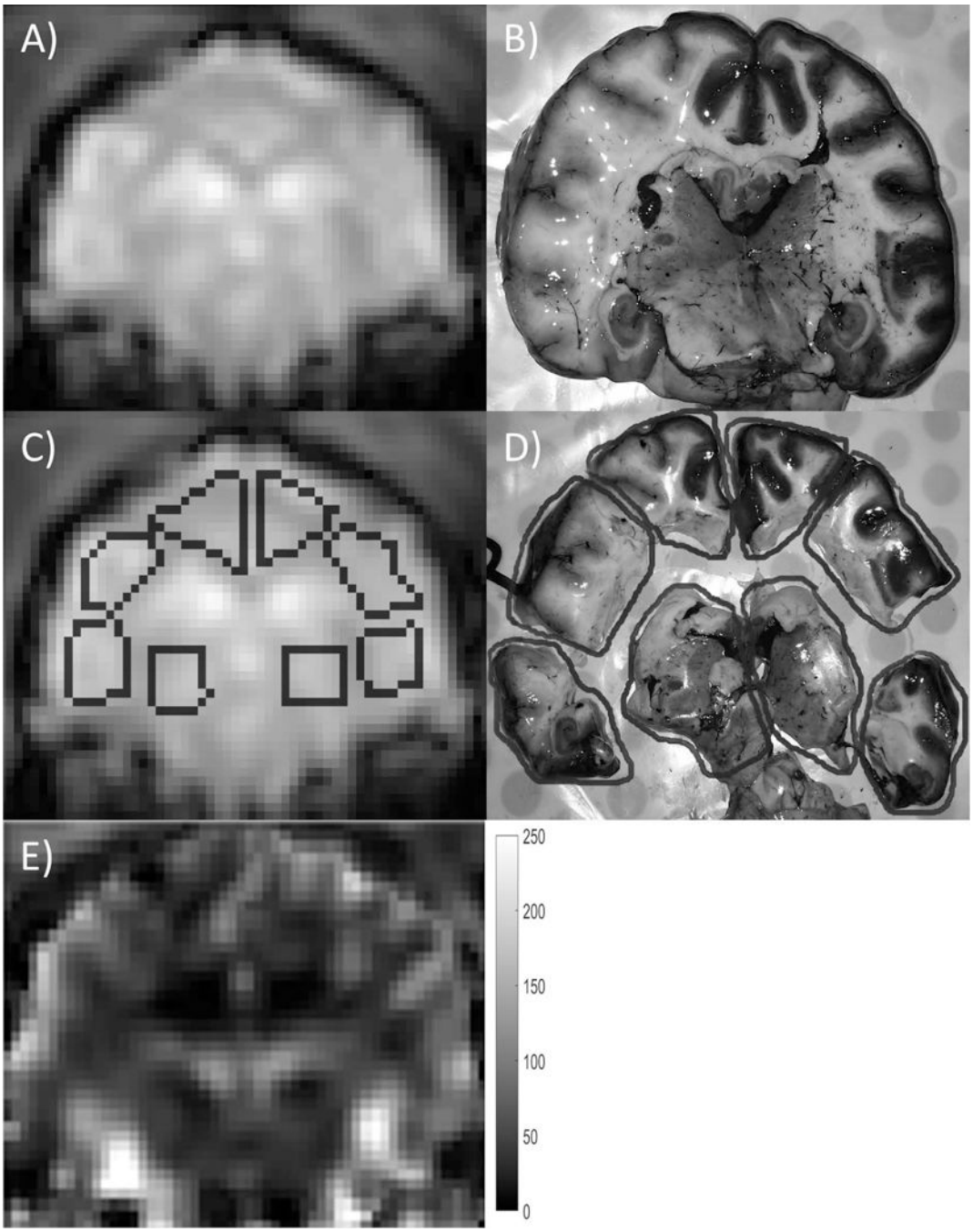

Figure 2.

Example of ROI registration between MRI and actual excised brain sections. Each slice was separated into eight regions, and corresponding ROIs were drawn on the MRI DSC images. The MRI DSC image (A, C) and photographic image (B, D) are shown with and without ROI contours (dark gray). The brain slice in (B) was cut into eight regions as shown in (D) for microsphere analysis. A qCBF (ml/100g/min) map of the same slice is shown in (E) for reference. In order to minimize bias, the ROIs were drawn on the DSC image prior to any knowledge of the qCBF map.

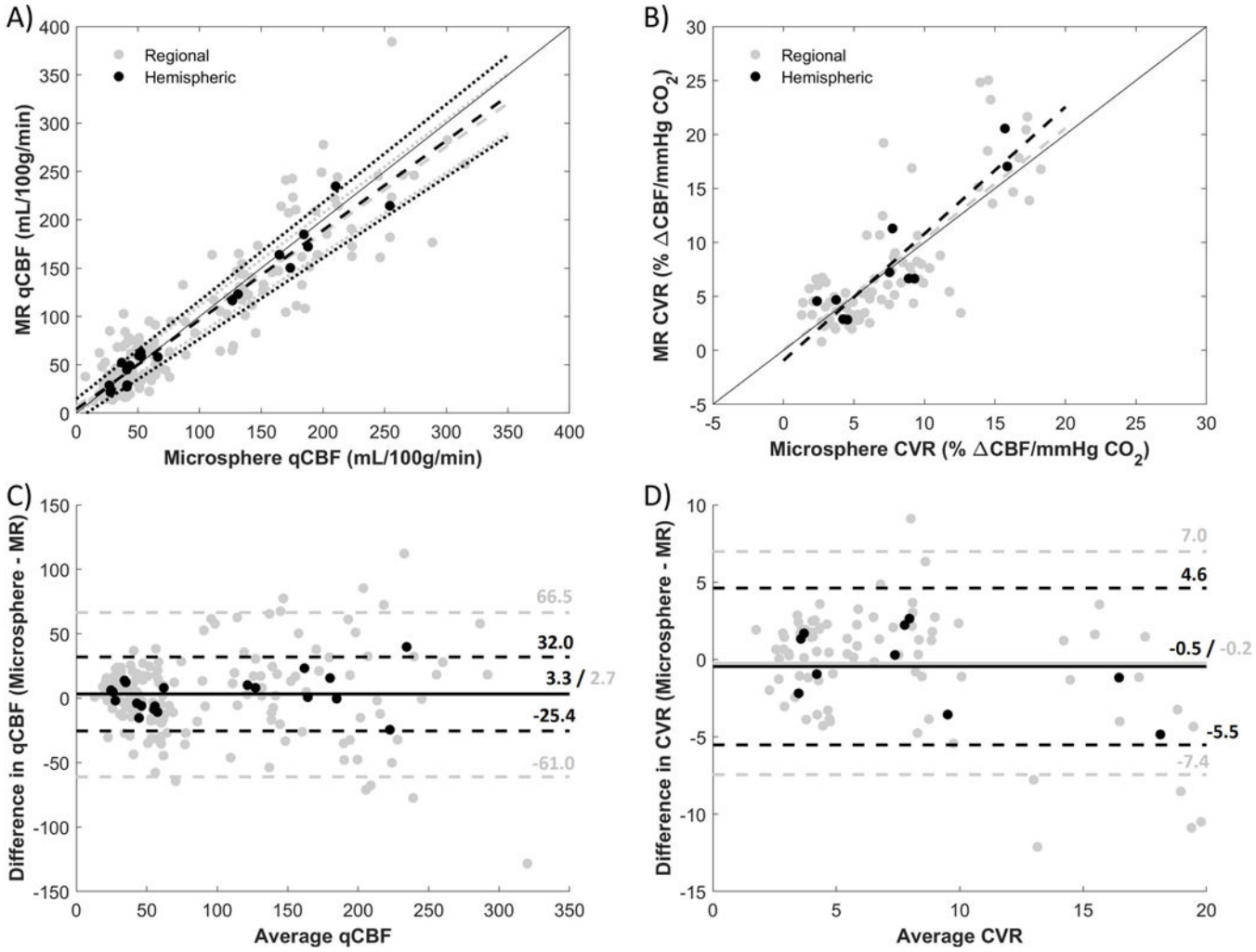

Figure 3.

Correlation and Bland-Altman plots of MR against microspheres for qCBF and CVR. In the correlation plots of A) qCBF and B) CVR, regional averages are shown in gray and hemispheric averages are in black. Dashed lines are derived from linear regression analysis, dotted lines represent 95% CI, and a line of unity is shown for reference. In the Bland-Altman plots of C) qCBF and D) CVR, the bias is represented by a solid line and the dashed lines are the limits of agreement. Though bias is low in both cases, there is quite a bit of spread in the differences.

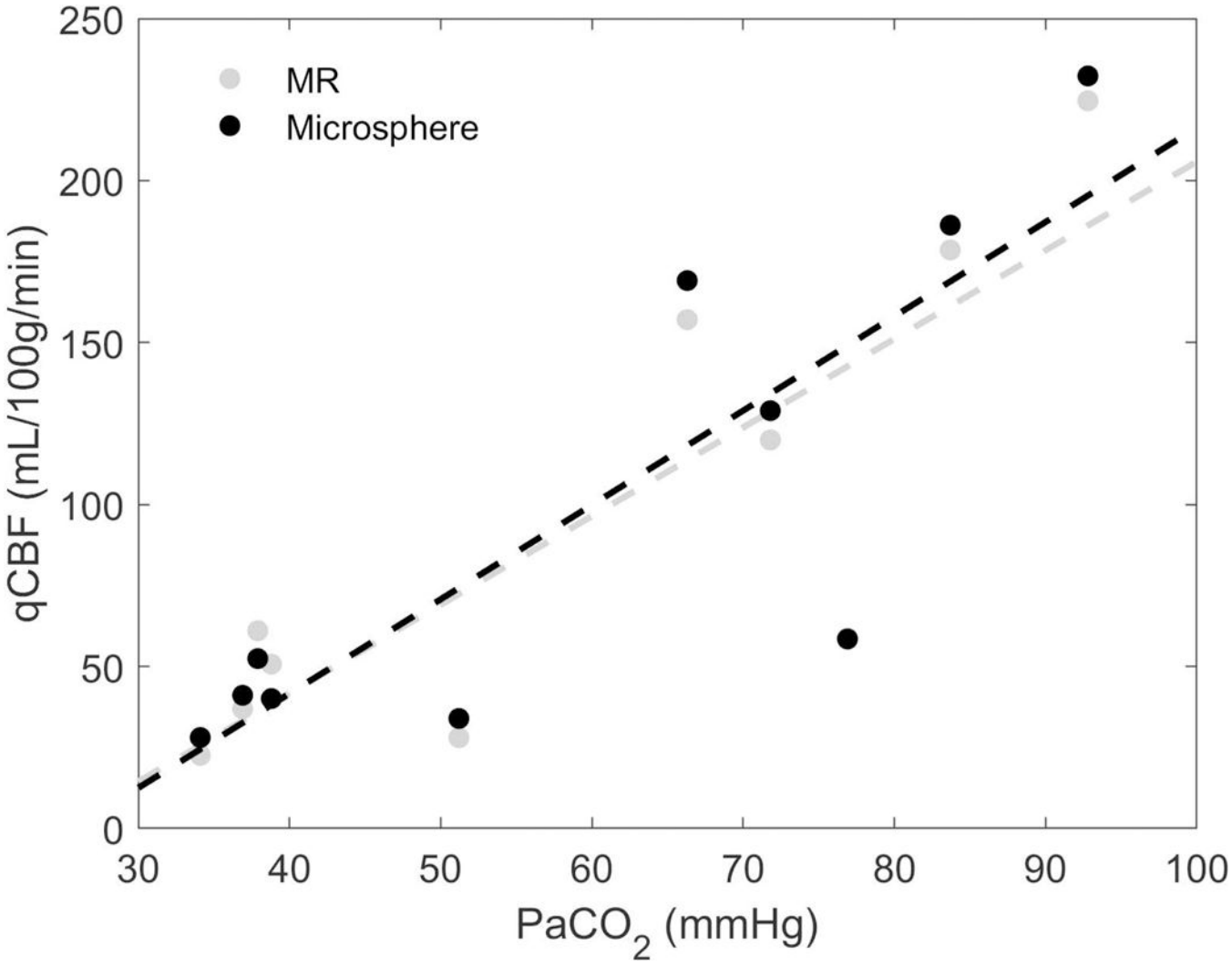

Figure 4.

Correlation plot of hemispheric averages of MR-qCBF (in gray) and microsphere-qCBF (in black) versus arterial $PaCO_2$. As expected, perfusion is increased with $PaCO_2$. Dashed lines are calculated by linear regression analysis.

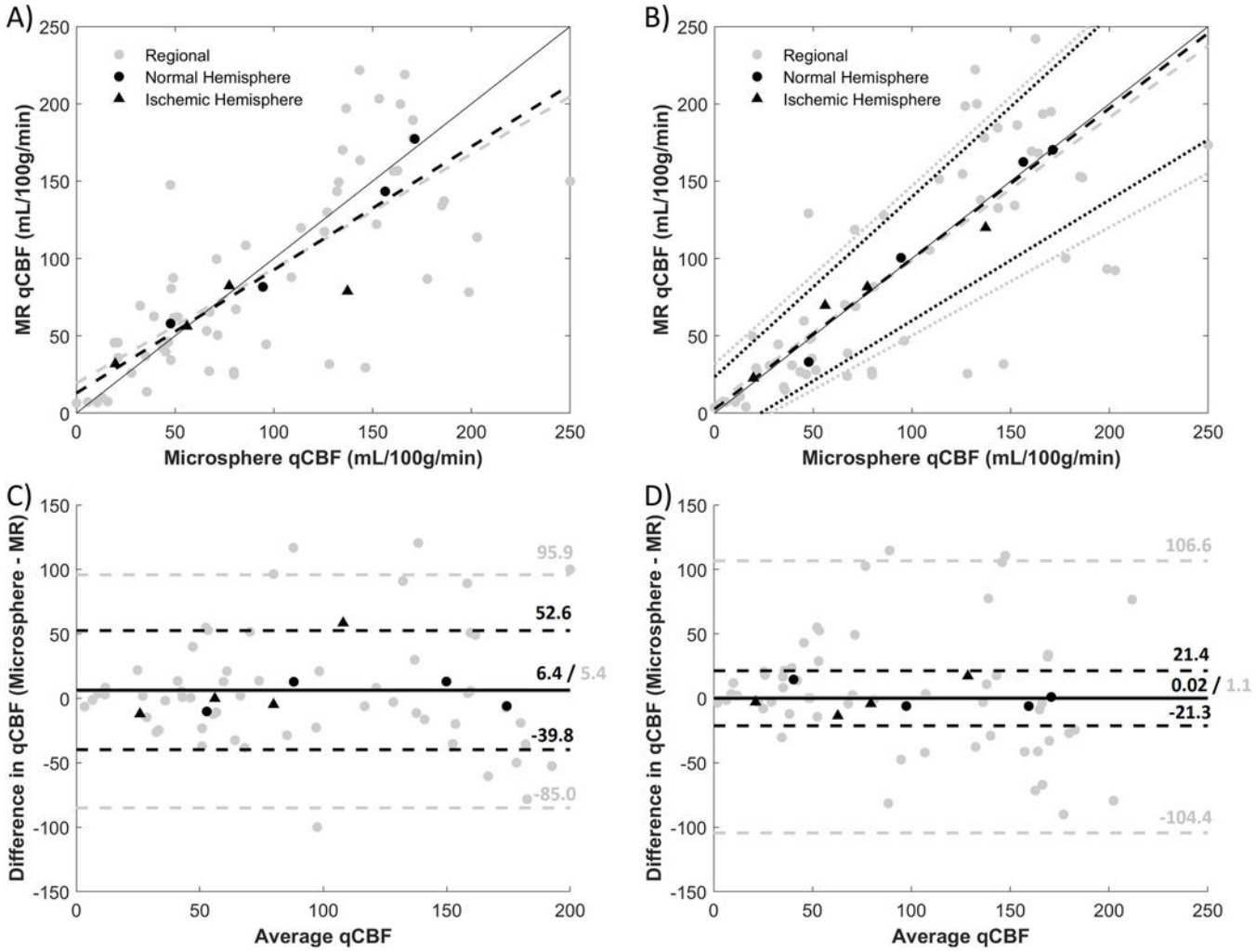

Figure 5.

Correlation and Bland-Altman plots of MR-qCBF vs. microsphere-qCBF with MCAO before (A, C) and after (B, D) delay and dispersion correction. Hemispheric averages are in black and regional averages are in gray. The hemispheres affected with MCAO are shown as triangles, while the contralateral sides are circles. Dashed lines are derived from linear regression analysis, dotted lines represent 95% CI, and a line of unity is shown for reference. An improvement in the hemispheric correlation can be seen after the correction, and the linear regression lines are brought closer to the line of unity. In the Bland-Altman plots (C, D), the bias is represented by a solid line and the dashed lines are the limits of agreement. After correction, the bias for hemispheric and regional are reduced closer to zero.

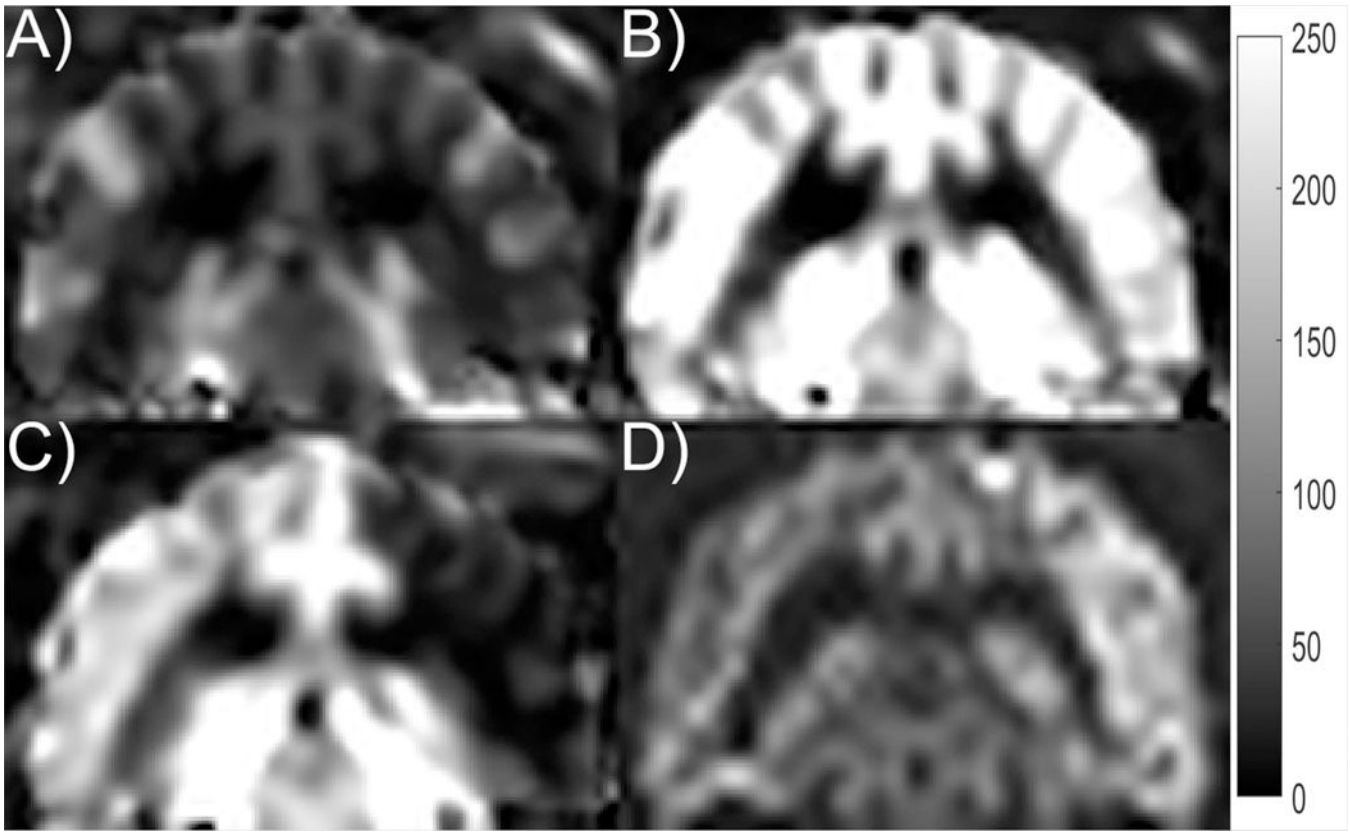

Figure 6.

Representative slice for (A) qCBF at normocapnia, (B) qCBF at hypercapnia, (C) qCBF with MCAO, and (D) DWI taken 2 hours after occlusion. The qCBF images are shown with a dynamic range of 0 to 250 ml/100g/min. The affected area in the (C) qCBF image with MCAO is shown as hypointense and is confirmed by the hyperintense area in the DWI. The unaffected hemisphere (left side of the image in C) is shown with high CBF despite normocapnia. This may have been due to increased usage of isoflurane during the longer experiment of day 2. The same effect was observed in the microspheres.

Table 1.

Linear regression results. For each analysis, the slope and intercept of the linear regression, its r^2 value, *P*-value, and 95% confidence intervals (CI) of the slope and intercept are reported.

Comparison	Linear regression	r^2	*P*	CI_{slope}	$CI_{intercept}$
qCBF MRI vs Spheres Hemispheric	$y = 0.93x + 3.85$	0.96	< 0.001	[0.84, 1.02]	[−6.9, 14.6]
qCBF MRI vs Spheres Regional	$y = 0.90x + 7.11$	0.82	< 0.001	[0.83, 0.96]	[−0.64, 14.9]
CVR MRI vs Spheres Hemispheric	$y = 1.17x - 0.95$	0.84	< 0.001	[0.76, 1.59]	[−4.74, 2.85]
CVR MRI vs Spheres Regional	$y = 1.03x - 0.04$	0.61	< 0.001	[0.85, 1.21]	[−1.48, 1.55]
qCBF MRI vs $PaCO_2$	$y = 2.73x - 67.6$	0.70	0.002	[1.29, 4.18]	[−158, 22.8]
qCBF Spheres vs $PaCO_2$	$y = 2.91x - 74.8$	0.72	0.002	[1.42, 4.41]	[−168 18.7]
qCBF MRI vs Spheres Hemispheric; MCAO	$y = 0.80x + 12.9$	0.82	0.002	[0.43, 1.16]	[−26.8, 52.7]
qCBF MRI vs Spheres Regional; MCAO	$y = 0.74x + 19.3$	0.54	< 0.001	[0.56, 0.92]	[−1.4, 40]
qCBF MRI vs Spheres Hemispheric; MCAO; DD corr	$y = 0.97x + 2.58$	0.96	< 0.001	[0.78, 1.17]	[−18.2, 23.4]
qCBF MRI vs Spheres Regional; MCAO; DD corr	$y = 0.93x + 5.93$	0.55	< 0.001	[0.70, 1.15]	[−19.8, 31.7]

MCAO – middle cerebral artery occlusion; DD corr – delay and dispersion correction

Table 2.

Summary of qCBF, CVR, and $PaCO_2$ for each case. MR and microsphere qCBF and CVR are listed as whole-brain averages. For qCBF and $PaCO_2$, pre- and post-stress values are presented as “pre / post”.

	qCBF (ml/100g/min)		CVR (% ΔqCBF per mmHg)		$PaCO_2$ (mmHg)
	MR	Microsphere	MR	Microsphere	
1	61.0 / 119.9	52.4 / 129.0	2.9	4.4	37.9 / 71.8
2	32.5 / 181.8	40.3 / 185.1	11.6	7.8	36.9 / 83.7
3	50.7 / 224.6	40.1 / 232.3	6.6	9.1	38.8 / 92.8
4	28.0 / 58.8	33.9 / 58.5	4.6	3.1	51.2 / 76.9
5	28.0 / 191.0	26.8 / 161.6	21.5	15.6	34.1 / 66.3